Structural and magnetic changes in FeNbCuSiB amorphous alloys during the crystallization process

1996 J. Phys.: Condens. Matter 8 5925

(http://iopscience.iop.org/0953-8984/8/32/012)

J. Phys.: Condens. Matter **8** (1996) 5925–5939. Printed in the UK

Structural and magnetic changes in FeNbCuSiB amorphous alloys during the crystallization process

P Gorria, J S Garitaonandia and J M Barandiarán

Departamento de Electricidad y Electrónica and ISEM, Universidad del Pais Vasco/EHU, Apartado 644, 48080 Bilbao, Spain

Received 5 February 1996, in final form 15 May 1996

Abstract. Calorimetric and magnetic measurements, x-ray powder diffraction and Mössbauer spectroscopy have been used to study the magnetic and structural changes occurring after each of the two steps of crystallization that take place in FeNbCuSiB-type alloys. Two samples with different boron and silicon concentrations, $Fe_{73.5}Nb_3Cu_1Si_{22.5-x}B_x$ ($x = 6, 9$), have been studied. They give a somewhat different composition of the crystalline phases appearing after crystallization processes. The most noticeable phenomenon is the observed increase of about 50 K in the Curie temperature of the FeSi crystalline phase between the end of the first crystallization process and the end of the second one, although the composition of this phase remains unchanged. This result is discussed in terms of crystal boundary effects. Also, the Curie temperature of the remaining amorphous phase, in the crystallized samples, is greater than the expected one, due to the coupling with magnetic phases with higher Curie points and inhomogeneities in such a phase.

1. Introduction

Nanocrystalline materials of $Fe_{73.5}Nb_3Cu_1Si_{22-x}B_x$ ($6 \leqslant x \leqslant 12$) type are very well known for their interesting magnetic properties, such as high permeability and saturation magnetization [1, 2]. They are usually obtained by isothermal heat treatments of the amorphous alloys at the appropriate temperatures and for periods of time between a few minutes and a few hours. Magnetic, calorimetric and electrical resistivity studies of such alloys reveal that the crystallization occurs in two steps [3, 4]. The first one corresponds to primary precipitation of a fcc FeSi phase with small crystal size (typical grain size diameter: 10–20 nm); at this stage, two different phases coexist in the alloy, the amorphous remaining matrix, enriched in boron and niobium, and the FeSi crystalline phase. Further heating degrades the soft magnetic properties. In the second crystallization step, the amorphous matrix gives rise to different FeB(Nb) crystalline phases [5] such as Fe_2B, Fe_3B or $Fe_{23}B_6$, FeNbB, depending on the percentage of B in the initial composition of the samples. For the two samples studied in this work, with $x = 6$ and 9, the two steps of the crystallization process are clearly separated by more than 100 K as seen in the DTA scans of figure 1. The occurrence of these Fe borides and other processes occurring at this stage, like the grain growth [6], greatly harden the FeSi magnetic phase.

Many studies related to the crystallization of these compounds have already been published [5, 7, 8, 9] but the diversity of heat treatments used by the different authors makes the comparison of the results difficult. In the present work, we have performed two different treatments of the samples in a DTA apparatus. The first one consists in heating up

0953-8984/96/325925+15$19.50

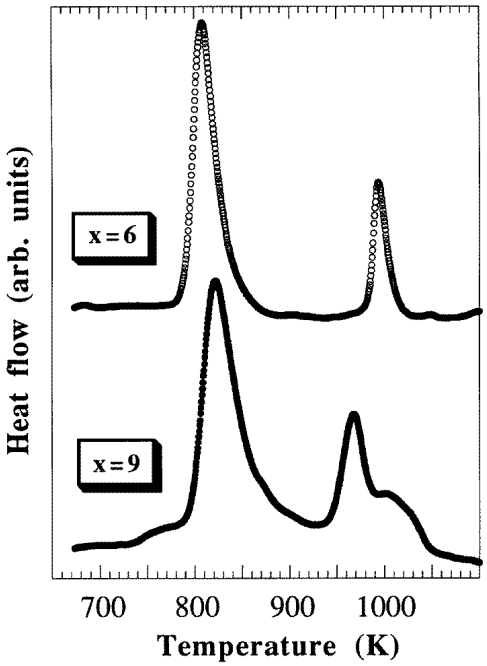

Figure 1. DTA curves for the two compositions studied: $Fe_{73.5}Nb_3Cu_1Si_{22.5-x}B_x$ ($x = 6$ and 9), showing the crystallization peaks.

the sample to a temperature above the end of the first crystallization step (≈923 K) and below the beginning of the second step. This treatment does not give the best magnetic properties, and, therefore, it has been less used than isothermal crystallization at lower temperatures. In the second treatment the samples were heated until the second crystallization was fully completed (1173 K). This procedure permits an independent study of the same sample after the two different crystallization processes and ensures that these processes have been fully completed. We have also performed two additional isothermal treatments of the $x = 9$ sample, one at 823 K for one hour, and a second one at 1223 K for one hour, to compare with the non-isothermally heated samples. Because these materials are composed of different magnetic and structural phases, they are ideal systems for investigating the magnetic interactions between the different phases.

Recently, the evolution of the Curie temperature of the amorphous phase remaining after the nanocrystallization in FeNbCuB alloys has been investigated [10]. Such alloys are similar to those studied in the present paper except for the lack of Si. The study in [10] reveals an increase of about 100 degrees in the value of T_C compared to that of the amorphous samples with the same composition. This increase has been interpreted as a result of the exchange-field penetration coming from the nanocrystalline Fe phase, a penetration which overcompensates the expected decrease of T_C due to compositional changes during nanocrystallization. Other authors [11] argued that the diffusion processes occurring during the crystallization lead to a sharp iron concentration gradient in the amorphous interphase, so slow-diffusing Nb atoms are rejected from FeSi forming crystallites, and the Fe-rich intergranular zones could have a greater T_C. In the compositions studied in this work, the same increase of T_C is observed. We have also observed that the Curie temperature of the

FeSi crystalline phase increases by about 50 K between the two crystallization processes, without any apparent change in the composition and amount of this phase.

In the following, to clarify the explanation of the results obtained, we shall call the $x = 6$ and $x = 9$ as-quenched samples B6/aq and B9/aq, the sample with $x = 9$ annealed for one hour at 823 K B9/0 (standard heat treatment used for obtaining optimal soft magnetic properties), the samples with $x = 6$ and $x = 9$ heated up below the second crystallization temperature B6/1 and B9/1, the fully crystallized samples with $x = 6$ and $x = 9$ B6/2 and B9/2, and the $x = 9$ sample annealed for one hour at 1223 K B9/3.

2. Experimental procedure

$Fe_{73.5}Nb_3Cu_1Si_{22.5-x}B_x$ ($x = 6, 9$) amorphous ribbons of 2 mm $\times$ 20 μm cross section were obtained from Vacuumschmelze. Annealing of the samples and calorimetric measurements were performed in a differential thermal analyser (DTA) at heating a rate of 20 K min^{-1}.

X-ray powder diffraction (XRD) patterns were obtained with Cu Kα radiation. The peaks corresponding to an α-Fe polycrystalline foil were also analysed in order to determine instrumental corrections. The data obtained by this technique were used to identify the different crystalline phases as well as the average grain size diameter and the lattice parameter of the FeSi phase.

Magnetic measurements were performed in a Manics DSM-8 Faraday magnetometer at $H_{app} = 80$ kA m^{-1}. The measurements of magnetization versus temperature, $M(T)$, were performed in three different temperature ranges, depending on the degree of crystallization of the samples, to obtain the T_C-values of the different ferromagnetic phases. Care was taken not to heat the partially crystallized samples above the temperatures of the previous treatments, so that no further crystallization occurs. The three temperature ranges used for these measurements of $M(T)$ are the following: between room temperature and 673 K for the as-quenched samples to measure T_C for the starting amorphous phase; between room temperature and 873 K for the partially crystallized samples, to obtain T_C(FeSi), and between room temperature and 973 K in the fully crystallized samples to obtain T_C(FeSi) and T_C(Fe borides).

Table 1. Curie temperatures, lattice parameters, Si contents and average hyperfine fields of the FeSi phase, after the two crystallizations, obtained from the different measurements (the estimated errors in the XRD results are between parentheses).

	T_C (K)			Si (at.%)			T_C (K) (estimated)
Samples	(a)	(b)	a (Å)	(c)	(d)	$\langle B_{HF} \rangle$ (T)	(e)
B6/1	840	835	5.670(5)	20.0(2)	20(1)	26.1	895
B9/1	850	860	5.675(5)	18.8(2)	19(1)	26.6	910
B6/2	888	890	5.680(5)	19.5(2)	19(1)	26.2	900
B9/2	910	920	5.685(5)	18.1(2)	18(1)	27.1	920

(a) From measurements of $M(T)$.
(b) From DTA measurements.
(c) From Mössbauer measurements.
(d) From XRD measurements.
(e) From Si percentages.

The Mössbauer spectra of the samples were obtained at room temperature in the transmission geometry using a conventional constant-acceleration spectrometer with a 512

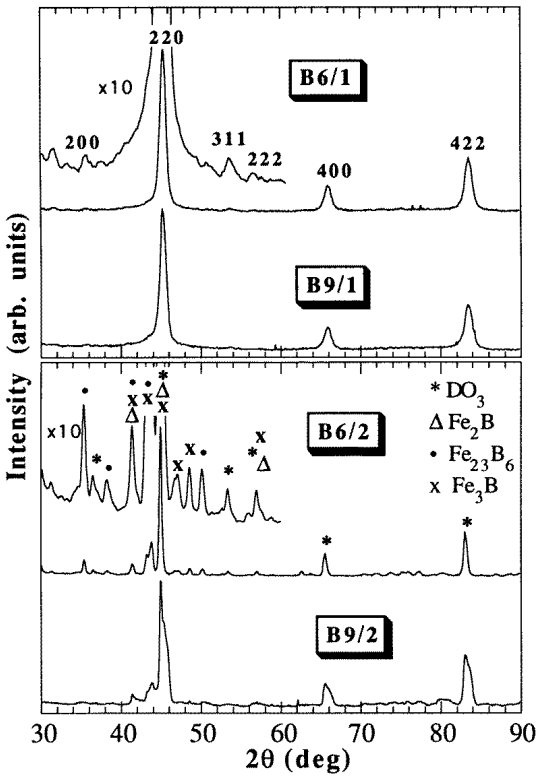

Figure 2. XRD patterns of the samples studied.

multichannel analyser and a ^{57}Co–Rh source. This technique was used to gain information about iron-containing phases and the relative percentages of these phases in the samples.

3. Results

3.1. XRD measurements

Figure 2 shows the XRD patterns of the heat-treated samples. It is well known that the structure of FeSi crystalline alloys depends on the percentage of Si [12]. For Si percentages below 10 at.% the structure is a disordered bcc solid solution with Si atoms substituting for iron. In the Si concentration range between 10 and 30 at.%, the structure is the DO_3-ordered fcc structure, and the lattice parameter is approximately twice that of the bcc solid solution. In the XRD patterns, peaks at the same position as those of bcc-Fe and additional peaks corresponding to the DO_3 superstructure may be observed. In the four patterns in figure 2, a few small peaks, which can be associated with this superstructure, appear. From XRD measurements we have calculated the lattice parameters of the FeSi phase by means of the $\cos\theta \operatorname{cotan}\theta$ method using the (220), (400) and (422) diffraction peaks [13]. The Si percentage in the FeSi phase corresponding to these lattice parameter values has been obtained from [14]. The values can be found in table 1. The XRD patterns have also been used to estimate the average grain size of the FeSi crystals.

Sample B6/1 shows only the diffraction peaks corresponding to the FeSi phase, but in B9/1 additional small peaks corresponding to Fe_2B can be identified. In both spectra there is a small broadening in the base of the (220) peak of the FeSi phase, due to the remaining amorphous matrix. For these samples the average grain size diameter of the FeSi nanocrystals, calculated from the peak width using the Scherrer formula [13], is about 20 nm.

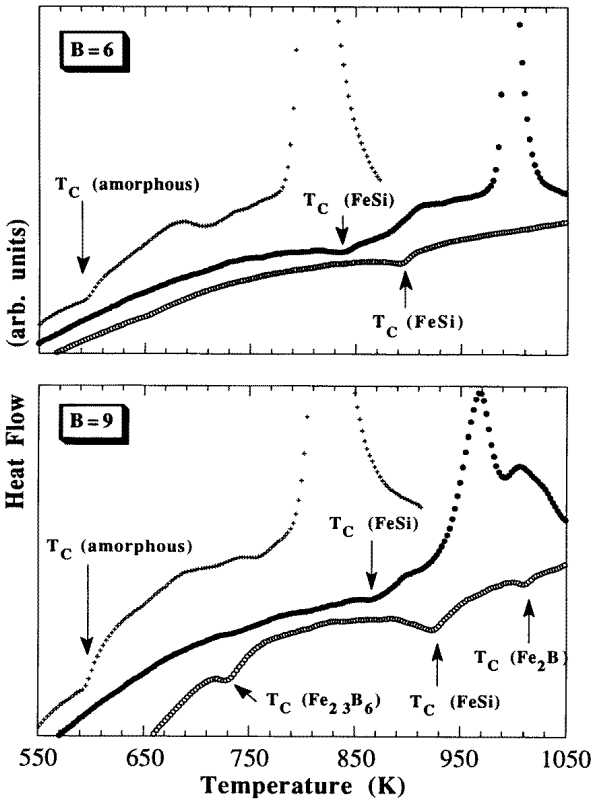

Figure 3. DTA curves for the samples (from top to bottom) B6/aq, B6/1, B6/2, B9/aq, B9/1 and B9/2 showing the treatments and the Curie temperatures of the different ferromagnetic phases.

In the XRD patterns of B6/2 and B9/2 new diffraction peaks appear; the most intense ones correspond to $Fe_{23}B_6$ [5] in the B6/2 sample and to Fe_2B and $Fe_{23}B_6$ in the B9/2 sample. A very small amount of Fe_3B could also be present in both samples. All of the peaks, including the FeSi peaks, are now sharper, indicating that the grain size of the crystallites is greater than in the B6/1 and B9/1 samples. However, it is difficult to calculate the size of the crystals because there are a mixture of peaks superimposed and it is not easy to isolate the contribution of each crystalline phase to the diffraction peaks, except in the 400 and 422 reflections of the DO_3 phase in the B6/2 sample. Data obtained from TEM experiments by other authors [6] give values greater than 100 nm for the FeSi grains, in samples thermally treated at temperatures above the crystallization of the Fe borides, in good agreement with the minimum value of 80 nm that we have estimated from the (400) and (422) reflections for B6/2.

3.2. Calorimetric and magnetic measurements

The DTA apparatus allows a continuous monitoring of the crystallization state of the samples as well as the measurement of the Curie temperatures. As shown in figure 1, two large irreversible exothermic peaks reveal the crystallization process. The first peak at ≈823 K corresponds to the crystallization of the FeSi phase with DO_3-type structure and the second one at ≈973 K is due to the crystallization of the iron borides. In contrast, Curie temperatures are shown by small reversible endothermic peaks (see figure 3). The measurements were made in several steps as follows: in the first one, the sample is heated from room temperature to the end of the first crystallization process and cooled down to room temperature. From the heat flow versus temperature curve obtained during this step, the value of T_C of the starting amorphous phase can be obtained. This sample will be used to perform further measurements. Later on, the first step is repeated with another ribbon of the same composition, which is later heated up from room temperature to 1173 K, a temperature at which the second crystallization process is completed. In this treatment, T_C for the nanocrystalline FeSi phase can be observed, but no peak corresponding to T_C for the remaining amorphous phase has been found. No evidence of any remaining first crystallization process is found. In the third step, the sample is cooled to room temperature and heated again to obtain T_C for FeSi and for Fe borides in the fully crystallized sample. The last heating stage also shows no evidence of further crystallization.

Calorimetric and magnetic measurements give very similar values of T_C for the FeSi phase in each sample and from these values we could make an independent estimation of the percentage of Si in this phase. However, we prefer to give T_C for the FeSi phase estimated from the percentages of Si obtained from structural studies like XRD and Mössbauer investigations (see table 1 for the values obtained), but in trying to do this we have encountered several difficulties. The most recently obtained Curie temperatures of FeSi alloys are given in [15]. However, later measurements on Fe_3Si [16] gave a value of T_C of 839 K for Fe_3Si, a value which is 35 K greater than the value given in [15]. This result is in clear agreement with the value of 835 K that we have obtained for an Fe_3Si sample prepared by us. So, we have assumed a value of 835 K for T_C for Fe_3Si and we have conveniently rescaled the results in [15], taking into account that the variation of the Curie temperature of $Fe_{100-x}Si_x$ compounds seems to be linear with the Si content in the range $12 \leqslant x \leqslant 25$. This fact allows us to perform an estimation of the value of T_C for the FeSi phase in our samples.

In figure 3 DTA curves for the samples B6/aq, B6/1 and B6/2 (upper part) and B9/aq, B9/1 and B9/2 (bottom part) are shown. In the B6/aq and B9/aq curves T_C for the amorphous phase is clearly observed, but it disappears from the other curves. Figure 4 shows the magnetization versus temperature curves for all of the samples. The coincidence in the values of T_C for the FeSi phase measured by the two techniques and the increase of the Curie point after the second crystallization step are evident in figure 4.

For B9/1, T_C for the FeSi phase is ≃855 K and there is no evidence of other Curie points. However, for the B9/2 sample four different Curie temperatures can be observed: T_C1 around room temperature, T_C2 between 600 and 700 K, T_C3 at ≃915 K and T_C4 above 973 K, which is the highest temperature attainable with the Faraday magnetometer. As already mentioned, peaks corresponding to three different crystalline phases, $Fe_{23}B_6$, FeSi and Fe_2B, have been identified in the XRD pattern of this sample. So, we assume that T_C2 corresponds to the $Fe_{23}B_6$ phase, T_C3 to the FeSi phase and T_C4 to Fe_2B. T_C1 should correspond to a Nb-rich phase whose Mössbauer subspectrum at room temperature seems to be paramagnetic, as is explained in the next section. The most noticeable result is the

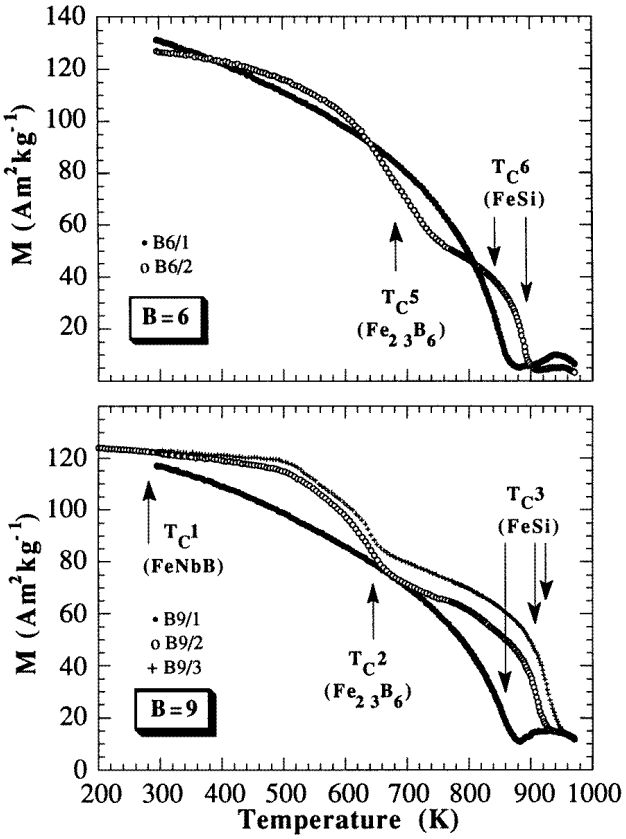

Figure 4. Magnetization versus temperature curves for the samples (from top to bottom) B6/1, B6/2, B9/1, B9/2 and B9/3. The Curie temperatures are marked by arrows.

increase by more than 50 K in the value of T_C for the FeSi phase.

The B6/1 sample shows a unique value of T_C of $\simeq$840 K, which corresponds to the Curie point of the FeSi phase. In the $M(T)$-curve of B6/2 two different Curie temperatures can be observed. The first one, T_C5 is between 600 and 700 K and does not appear clearly in the DTA curve. The second, T_C6 is $\simeq$890 K; however, the $M(T)$-curve (figure 4) does not drop to zero even at 973 K. Hence, some amount of Fe_2B phase with $T_C > 973$ K, could be present in the sample. The XRD pattern shows very clear peaks corresponding to an FeSi crystalline phase and $Fe_{23}B_6$. In this case, we associate T_C5 with $Fe_{23}B_6$ and T_C6 with FeSi. For this composition, the increase in T_C for the FeSi phase is about 50 K.

3.3. Mössbauer measurements

The fitting of the Mössbauer spectra has been performed with the NORMOS program, developed by Brand *et al* [17], a program which allows a simultaneous fit of several crystalline spectra and a possible amorphous phase characterized by a distribution of hyperfine fields (B_{HF}). The fittings have been done differently depending on the crystallization state of the samples. For the B6/1 and B9/1 samples the spectra have been fitted using the FeSi subspectra discussed below and a B_{HF}-distribution for the remaining

amorphous phase, whereas for the spectra of the B6/2 and B9/2 samples the fittings have been made taking into account all the crystalline phases, i.e. $Fe_{23}B_6$, Fe_2B, etc, discussed above.

For the fitting of the FeSi contribution to the spectra we have used information about FeSi crystalline phases and site denominations given by Stearns [18]. In order to be as clear as possible in the analysis of the results, we have assigned each subspectrum to a different Fe environment in all of the Fe-containing phases, since the nomenclature used by other authors is confusing [7, 9].

The structure of the FeSi crystalline phase is of the fcc DO_3 type, as is that of Fe_3Si. In this phase two different subspectra can be observed, corresponding to two different iron positions labelled A and D. The A positions are occupied only by Fe, with four Fe atoms and four Si atoms as nearest neighbours. The D positions, with eight Fe atoms as nearest neighbours, are equally occupied by Fe and Si. When the percentage of Si is lower than 25 at.%, some of the Si sites are occupied by Fe, and additional subspectra for the A sites appear, depending on the number of Fe nearest neighbours. These are labelled with Ai, $i = 4, 5, 6, 7, 8$ (the number of Fe atom nearest neighbours). The hyperfine fields, B_{HF}, of these subspectra increase with the number of Fe nearest neighbours. The probability of each Ai-subspectrum can be calculated using a binomial distribution [18]. These calculated probabilities are close to those obtained from the Mössbauer spectra (the difference is less than 4% for the B6/1 and B6/2 samples and less than 6% for the B9/0 and B9/2 samples, similar to the differences given in [18]), with the exception of the B9/1 sample, in which the difference between the calculated and experimental values reaches 17%. In our samples the percentage of Si in the FeSi phase is high but it remains below 25 at.%; therefore, the probability for the A8 and A7 subspectra is very low and we have neglected their contributions, which may be hidden by the D subspectrum. Furthermore, the Fe atoms in D positions experience the effect of the Fe next-nearest neighbours. Hence, different B_{HF}-values for the D Fe atoms are expected depending on the number of Fe next-nearest neighbours. In order to include this effect we have used two D subspectra in the fit. The first represents the D Fe atoms with a large number of iron next-nearest neighbours and the second represents the D Fe atoms with a small number of iron next-nearest neighbours. Hence, we have fitted the FeSi crystalline phase with five subspectra labelled, D, D′, A6, A5 and A4.

For each site in the DO_3 phase we can only vary the values of B_{HF}, the isomer shift (IS) and the quadrupole shift (QS), and this in a restricted range around the values found for pure FeSi alloys. The linewidths were held constant in a first step and allowed to vary in the second step, in order to improve the quality of the fit. However, they showed no appreciable increase, remaining very close to the values obtained for the calibration α-Fe foil (0.3 mm s^{-1}). The relative areas of the different lines of the fully crystallized B6/2 and B9/2 samples were allowed to vary in the fits. The area ratio obtained is $\simeq$2.6:1.9:1. Due to some restrictions in the amorphous fitting program, the area ratios of the 1 and 3 lines (D13) were fixed to the value obtained from the fitting of the fully crystallized samples, 2.6, and we have allowed the area ratio of the 2 and 3 lines (D23) to vary. The value obtained for D23 for the B9/0, B9/1 and B6/1 samples was always between 1.9 and 2, as for the B9/2 and B6/2 samples, which is typical for random orientation of the crystallites in a polycrystalline sample.

Even with such restrictions, the number of parameters in the fit, including the amorphous phase, was over 25. Hence, care should be taken in keeping the values obtained in a reasonable range. The values displayed in tables 2 and 3 reflect the good agreement between the parameters corresponding to the same subspectra in different samples, and give

Table 2. Hyperfine parameters, the linewidth (LW) and the percentage of Fe in each subspectrum obtained from the Mössbauer spectra for the $x = 6$ samples. (The IS is referred to the α-Fe calibration foil.)

Subspectra	B_{HF} (T)	QS (mm s^{-1})	IS (mm s^{-1})	LW (mm s^{-1})	% Fe (a)
D′ (B6/1)	32.3	0.03	−0.08	0.30	10
D′ (B6/2)	32.6	0.00	−0.09	0.29	6.8
D (B6/1)	31.1	0.01	−0.02	0.39	19.2
D (B6/2)	31.6	−0.01	−0.02	0.41	19.1
A6 (B6/1)	28.6	0.03	−0.01	0.40	11.9
A6 (B6/2)	28.7	0.00	−0.01	0.39	13.3
A5 (B6/1)	24.6	0.02	0.07	0.38	24.0
A5 (B6/2)	24.5	0.02	0.08	0.39	26.4
A4 (B6/1)	19.7	0.02	0.15	0.33	23.4
A4 (B6/2)	19.6	0.02	0.13	0.38	20.6
$Fe_{23}B_6$ (B6/1)	—	—	—	—	—
$Fe_{23}B_6$ (B6/2)	19.5	−0.15	−0.27	0.41	8.1
FeNbB (B6/1)	—	—	—	—	—
FeNbB (B6/2)	2.6	0.00	−0.07	0.51	5.7
Amorphous (B6/1)	—	—	−0.03	—	11.5
Amorphous (B6/2)	—	—	—	—	—

(a) Calculated from the relative area of the subspectrum.

confidence in the procedure used in the fit. The only appreciable difference is shown in the IS of Fe_2B: the value of this parameter changes from 0.08 mm s^{-1} for the B9/1 sample to −0.07 mm s^{-1} for the B9/2 sample; we are not able to interpret this variation, but taking into account that the total amount of this phase is lower than 10%, it is difficult to asseverate whether this is a real difference or not. Errors in the parameters, taken individually, are provided by the fitting program, and are extremely low. However, as a consequence of the number of parameters being fitted simultaneously, the actual uncertainty is greater. By comparing different sets of parameters which give very similar χ^2-values for the whole fit, we estimate such uncertainty in a few units in the last significant figure for each value in tables 2 and 3.

For the calculation of the Si content of the FeSi phase we have taken into account the resonant area of each Ai-subspectrum relative to the whole FeSi area and the number of Si atoms in each Ai-subspectrum. The percentage of Si in the FeSi phase thus obtained is given in table 1 together with the percentages obtained from XRD. In addition, we have measured the average hyperfine field of the FeSi phase in each sample (see table 1), and the different values of $\langle B_{HF} \rangle$ obtained are in clear accordance with the different Si percentages [18]. The percentage of FeSi crystalline phase obtained from the Mössbauer experiments is about 72–73 at.% for the $x = 9$ compound, in both the B9/1 and B9/2 samples. For the $x = 6$ composition, the percentage of FeSi does not change either during the second crystallization process, and the calculated value is about 81–82 at.%, in both the B6/1 and B6/2 samples. The percentages of each phase are summarized in table 4 for the B6/1, B6/2, B9/1 and B9/2 samples. These percentages have been determined from the normalized resonant area of each subspectrum, which is proportional to the amount of iron in each phase. If there are several subspectra corresponding to a unique phase we have to add the

Table 3. Hyperfine parameters, the linewidth (LW) and the percentage of Fe in each subspectrum obtained from the Mössbauer spectra for the $x = 9$ samples. (The IS is referred to the α-Fe calibration foil.)

Subspectra	B_{HF} (T)	QS (mm s^{-1})	IS (mm s^{-1})	LW (mm s^{-1})	% Fe (a)
D′ (B9/0)	32.4	0.01	−0.06	0.29	8.9
D′ (B9/1)	32.4	0.01	−0.07	0.30	10.9
D′ (B9/2)	32.4	−0.02	−0.06	0.32	17.7
D (B9/0)	31.1	0.02	−0.04	0.30	8.2
D (B9/1)	31.2	0.05	−0.05	0.38	15.0
D (B9/2)	31.1	0.07	−0.07	0.40	11.4
A6 (B9/0)	28.8	0.06	−0.02	0.33	7.9
A6 (B9/1)	28.6	0.02	−0.02	0.41	19.6
A6 (B9/2)	28.5	−0.02	−0.01	0.41	16.6
A5 (B9/0)	24.4	0.01	0.08	0.31	12.6
A5 (B9/1)	24.7	0.03	0.07	0.33	15.0
A5 (B9/2)	24.0	0.03	0.09	0.34	23.7
A4 (B9/0)	19.6	0.01	0.15	0.31	12.4
A4 (B9/1)	19.5	0.03	0.15	0.39	19.8
A4 (B9/2)	19.2	0.05	0.15	0.36	11.2
$Fe_{23}B_6$ (B9/0)	—	—	—	—	—
$Fe_{23}B_6$ (B9/1)	—	—	—	—	—
$Fe_{23}B_6$ (B9/2)	18.3	−0.17	−0.22	0.41	3.9
Fe_2B (B9/0)	—	—	—	—	—
Fe_2B (B9/1)	23.8	−0.01	0.08	0.32	6.4
Fe_2B (B9/2)	23.5	0.02	−0.07	0.29	8.0
FeNbB (B9/0)	—	—	—	—	—
FeNbB (B9/1)	—	—	—	—	—
FeNbB (B9/2)	—	0.00	−0.05	0.51	7.4
Amorphous (B9/0)	—	—	−0.02	—	50.1
Amorphous (B9/1)	—	—	−0.05	—	13.3
Amorphous (B9/2)	—	—	—	—	—

(a) Calculated from the relative area of the subspectrum.

Table 4. The percentages of each of the crystalline phases in the samples studied determined from Mössbauer measurements.

Samples	% amorphous	% FeSi	% Fe_2B	% $Fe_{23}B_6$	% FeNbB
B6/1	17.5	81.5	—	—	—
B6/2	—	81.5	—	7.5	10
B9/1	20	72.5	6.5	—	—
B9/2	—	72.5	9	4	13.5

amount of iron calculated from each subspectrum. Finally, the percentage of each phase is determined taking into account the composition of the phase and the previously calculated amount of iron.

In addition to the FeSi phase, the analysis of the spectra corresponding to the B6/1 and B9/1 samples (see figure 5) reveals an amorphous phase, whose hyperfine-field distributions

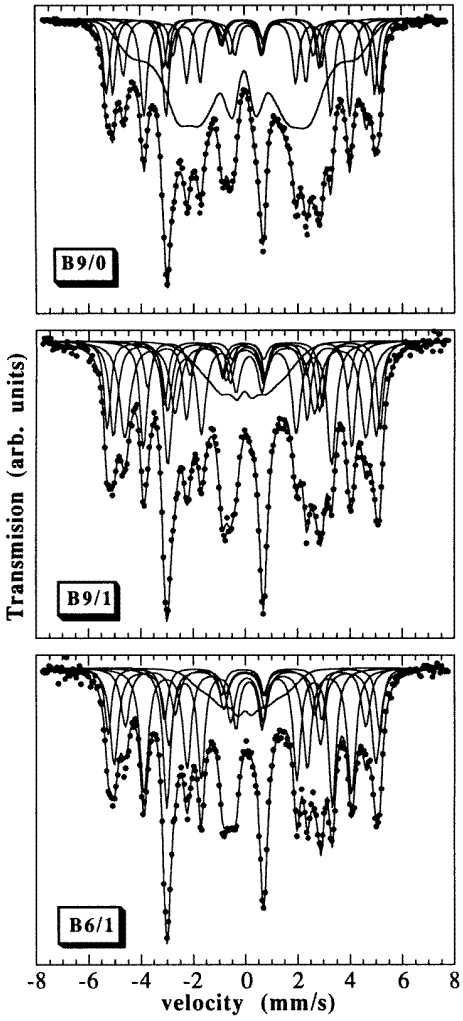

Figure 5. Mössbauer spectra and their fits for the (from top to bottom) B9/0, B9/1 and B6/1 samples.

have two maxima (see figure 6). In the B9/1 sample there is also evidence of a small amount of Fe_2B. In figure 5 the spectrum of the B9/0 sample is also presented for comparison with the spectra of the samples in which the first crystallization process is completed. In this figure it can be observed that the amount of remaining amorphous phase in the B9/0 sample is greater than in B9/1. Taking into account the calculated percentage and composition of the crystalline phase(s) in the B6/1 and B9/1 samples, we assume that the composition of the remaining amorphous phase is close to Fe_3NbB_2. The hyperfine-field distributions for the remaining amorphous phase in the B6/1 and B9/1 samples is compared with the distribution for the B9/aq and B9/0 samples in figure 6. The shape of the B9/0 distribution reveals the compositional inhomogeneities in the amorphous matrix due to the nanocrystallization process. As the nanocrystallization process goes on, the amorphous matrix becomes poorer in Fe, and the average B_{HF} decreases as already discussed in [19]. However, for B9/0, we found that some Fe atoms remain at the highest B_{HF}, indicating the existence of Fe-rich zones, probably arising from the concentration gradient above [11]. The existence of these Fe-rich zones with high B_{HF} are also corroborated by the increase of about 40 K in T_C for

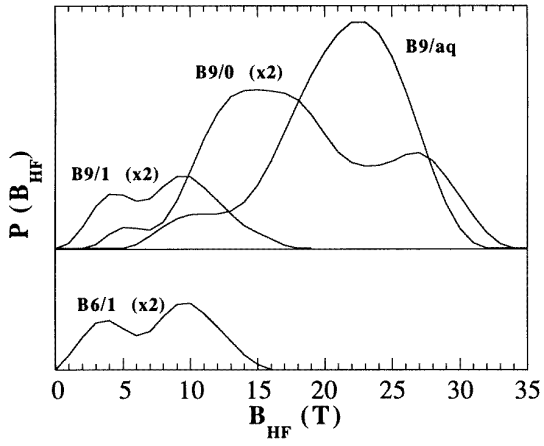

Figure 6. Hyperfine-field distributions of the amorphous remaining phase in the samples B9/0, B9/1 and B6/1 compared with the B9/aq sample.

the amorphous phase compared to the value measured for the as-quenched sample. Finally, when the first crystallization process is completed, the average hyperfine-field distribution of the remaining amorphous phase shows two different maxima at 4 and 10 T (see figure 6), which clearly indicate that the amorphous matrix is very inhomogeneous and poor in Fe.

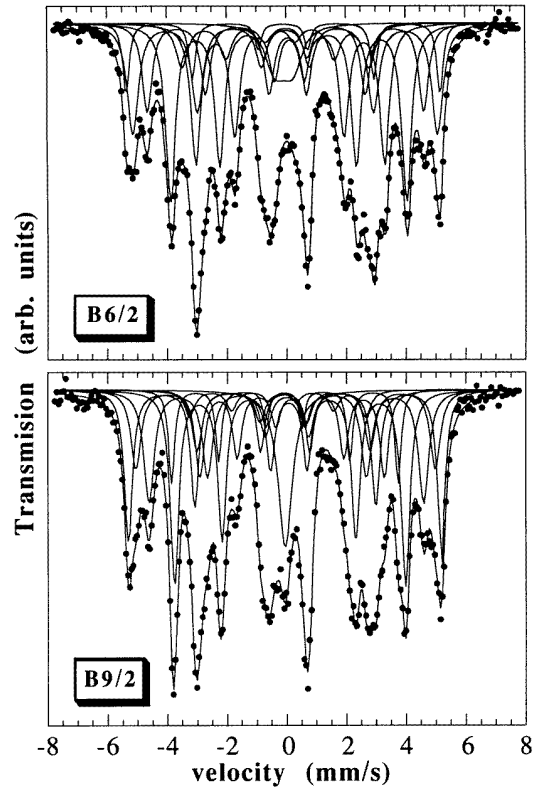

Figure 7. Mössbauer spectra and their fits for the B6/2 (top) and B9/2 (bottom) samples.

To satisfactorily fit the B6/2 and B9/2 Mössbauer spectra, additional subspectra are needed [20] (see figure 7). For the B9/2 sample we have found about 9–10% of Fe_2B, but there is no evidence of this phase in the B6/2 sample. In both samples there is some amount of the $Fe_{23}B_6$ phase (≈7.5% in B6/2 and ≈4% in B9/2), and 10–13 % of another phase already observed by other authors [7, 21], a phase which seems to be paramagnetic at room temperature. This phase has a Curie temperature near room temperature as was pointed out before, and the approximate composition could be equiatomic FeNbB. Only crystallographic data for this phase have been found [22], and to the authors' knowledge no information about its magnetic properties has been reported. The exact composition of this phase is not determined and small differences in Nb content could lead to small changes in T_C. Hence, because the value of T_C is around room temperature these changes could be responsible for the different shapes of the two subspectra in B6/2 and B9/2. The subspectrum in B9/2 corresponds to a paramagnetic phase, and for B6/2 it is broader and could correspond to an ordered phase with $B_{HF} \approx 2.6$ T, at the temperature of the Mössbauer experiments (see table 2).

We have not included any subspectrum corresponding to Fe_3B for the B6/2 and B9/2 samples, nor any subspectrum corresponding to Fe_2B for the B6/2 samples, because the percentage of these phases is smaller than 3% and it is at the experimental threshold. Hyperfine parameters and the percentages of iron of each of the subspectra are summarized in table 2 for the $x = 6$ samples and in table 3 for $x = 9$ samples.

4. Discussion

In the B6/1 and B9/1 samples some amorphous phase still remains, but as shown by the two maxima in the hyperfine-field distributions, at 4 and 10 T (see figure 6), this amorphous phase is not homogeneous. The inhomogeneities in the intergranular amorphous phase could come from the nanocrystallization process. In this process, the different diffusion coefficients of the elements and the rejection of Nb atoms from the FeSi crystallites [23] lead to compositional gradients in the amorphous matrix [11]. Hence, the structure of the amorphous matrix could be divided into Nb-rich regions close to the FeSi interphases and Fe-rich ones in the bulk matrix, and both regions would have different values of T_C and $\langle B_{HF} \rangle$. Tentatively, the small hyperfine-field contribution could be assigned to the Nb-rich zones and the large hyperfine-field contribution to the Fe-rich zones [19].

The existence of inhomogeneities in the amorphous matrix is also supported by the absence of any clear slope change in the $M(T)$-curves at temperatures below 773 K, and several Curie points could lie in this temperature range. Further, the endothermic peak associated with T_C for the remaining amorphous phase in the DTA curves (see figure 3), has actually disappeared as the amount of this phase has decreased and the inhomogeneity has become very large. If the approximate composition of the remaining amorphous phase is, as we have mentioned in the above section, Fe_3NbB_2, its Curie temperature extrapolated from the results in [10] should lie below room temperature. The separation of the amorphous matrix into two different phases could increase the value of T_C of one of them, at the expense of the other one, but in our case the two possible phases present in the amorphous matrix are ferromagnetic at room temperature, so exchange coupling enhancement, produced by the FeSi crystallites, must be present [10].

From the Mössbauer measurements, the calculated Si percentages in the FeSi phase at this stage are 20% and 18.8% for B6/1 and B9/1 respectively. The values of T_C for FeSi pure alloys with these Si percentages are 895 K and 910 K respectively, but the measured values are only 840 K for B6/1 and 855 K in B9/1. These percentages of Si cannot be

underestimated because they coincide approximately with the maximum possible amount of Si taking into account the number of Fe atoms in the FeSi phase and the total number of Si atoms in the sample. However, the Curie temperature of the FeSi phase for the B6/1 and B9/1 samples is lower than expected. The latter result could be explained in terms of defects in the FeSi grains. Due to the small size of the crystallites a large number of atoms lie at the surface and 'feel' lower magnetic exchange coupling than the bulk atoms. In addition, the heat treatment leading to the crystallization has been rapid and there has probably been no time to stabilize an FeSi phase with exactly the same percentage of Si in all the FeSi crystals. This fact, together with the effect of the surface atoms and inner defects in the nanocrystals, can be responsible for the broadening and worse definition of the T_C endothermic peak shown in the DTA curves.

On heating the samples above 900 K, new crystalline phases appear, namely the phases $Fe_{23}B_6$ and FeNbB, which seem to be the products of the crystallization of the remaining amorphous phase. The results obtained for the two compounds studied show that the percentage of FeSi crystalline phase does not change between the end of the first crystallization process and the end of the second one. The percentage of Si in this phase slightly decreases (see table 1), as can be concluded from the values of the resonant area and hyperfine parameters of each subspectrum. These small changes in the Si percentage could lead to changes in the Curie temperature of the FeSi phase no larger than 6 and 8 K for the $x = 6$ sample and for the $x = 9$ sample, respectively. In contrast, changes about 50–60 K in the value of T_C of FeSi are observed during the second crystallization process. The DTA peak associated with the transition is now sharp and well defined, indicating the annealing out of the defects in the FeSi phase. This crystallization process is accompanied with a substantial increase of the grain size, thus decreasing the number of surface atoms in each crystal. For the B6/2 and B9/2 samples, T_C for FeSi reaches 890 and 915 K; these values are approximately 10–15 K lower than the expected ones for these Si percentages.

In addition to these treatments, as we have mentioned before, a piece of $x = 9$ ribbon was heated at 1223 K for one hour, to stabilize the crystalline phases at a temperature at which all crystallization processes are completed (sample B9/3). In this case, the amount of FeSi phase is the same as in the B9/2 sample and the percentage of Si too, but T_C for FeSi again increases its value by 10 K, up to $\simeq$925 K, in agreement with the value of T_C for an FeSi alloy with 18 at.% Si. This increase in the Curie temperature is unlikely to arise from interactions due to the presence of a magnetic phase, Fe_2B, with a higher value of T_C (1013 K) than FeSi, as the FeSi grain size has greatly increased to about 0.1 μm in size, and the exchange is not likely to penetrate more than a few nanometres into the crystals [24]. Other effects due to the presence of Fe_2B crystals, such as dipolar interactions, will not increase the value of T_C(FeSi) by more than 1.5–2 K. Hence, we assume that the increase of the value of T_C of FeSi up to the expected value (925 K for 18 at.% in Si) is due to the effect of the isothermal heat treatment, which homogenizes the composition of the FeSi crystals and minimizes the amount of defects in the sample.

5. Conclusions

From accurate Mössbauer and XRD measurements on nanocrystalline alloys, we can conclude that the amount of crystalline FeSi phase is different in each composition, but does not change between the end of the first crystallization process and the full crystallization of the samples. These measurements also show that the percentage of Si in this phase remains almost unchanged and is approximately equal to the total amount of Si present in the original alloy.

The increase of the value of T_C for the remaining amorphous phase, above the expected value, is due to both compositional inhomogeneities in the amorphous matrix and the exchange-field penetration from the FeSi nanocrystallites.

However, the Curie temperature of the FeSi phase is lower than expected in the samples crystallized at temperatures below the beginning of the second crystallization process. This degradation of the magnetic properties has been interpreted in terms of the existence of defects in the FeSi nanocrystals and a great number of atoms in the amorphous–nanocrystal interphase. The crystallization of the amorphous matrix and the growth of the FeSi crystals, above 100 nm in size after the second crystallization process, make the interphase defects less significant due to the smaller ratio between the number of atoms in the interphase and the number of atoms in the bulk. During the second crystallization process of the samples T_C for FeSi increases its value by 50–60 K.

Acknowledgments

This work was supported by the Spanish CICYT under grant MAT93-0691. Two of the authors (PG and JSG) wish to thank the Basque Government for financial support under a FPI grant. We also want to thank Dr G Herzer for kindly supplying the samples and Dr I Orue for helpful discussions and for Fe_3Si sample preparation.

References

[1] Yoshizawa Y, Oguma S and Yamauchi K 1988 *J. Appl. Phys.* **64** 6044
[2] Herzer G 1993 *Phys. Scr.* T **49** 307
[3] Herzer G and Warlimont H 1992 *Nanostruct. Mater.* **1** 263
[4] Barandiarán J M, Fernández Barquín L, Gómez Sal J C, Gorria P and Hernando A 1993 *Solid State Commun.* **88** 75
[5] Allia P, Baricco M, Tiberto P and Vinai F 1992 *Studies of Magnetic Properties of Fine Particles and their Relevance to Material Science* ed J L Dormann and D Fiorani (Amsterdam: Elsevier Science) p 411
[6] Herzer G 1990 *IEEE Trans. Magn* **26** 1397
[7] Rixecker G, Schaaf P and Gonser U 1992 *J. Phys.: Condens. Matter* **4** 10 295
[8] Gorria P, Orúe I, Plazaola F and Barandiarán J M, 1993 *J. Appl. Phys.* **73** 6600
[9] Zbroszczyk J 1993 *Phys. Status Solidi* a **136** 545
[10] Hernando A, Navarro I and Gorria P 1995 *Phys. Rev.* B **51** 3281
[11] Yavari R 1995 *Nanostructured and Non-crystalline Materials* ed M Vázquez and A Hernando (Singapore: World Scientific) p 35
[12] Kubaschewski O 1982 *Iron Binary Phase Diagrams* (Berlin: Springer)
[13] Cullity B D 1967 *Elements of X-Ray Diffraction* (New York: Addison-Wesley) p 330
[14] Bozorth R M 1951 *Ferromagnetism* (Princeton, NJ: Van Nostrand) p 74
[15] Chin G Y and Wernick J H 1986 *Ferromagnetic Materials* vol 2, ed E P Wohlfarth (Amsterdam: North-Holland) p 78
[16] Niculescu V, Raj K, Budnick J I, Burch T J, Hines A and Menotti A H 1976 *Phys. Rev.* B **14** 4160
[17] Brand R A, Lauer J and Herlach D M 1984 *J. Phys. F: Met. Phys.* **14** 555
[18] Stearns M B 1968 *Phys. Rev.* B **168** 588
[19] Miglierini M 1994 *J. Phys.: Condens. Matter* **6** 1431
[20] Navarro I 1994 *PhD Thesis* Universidad Complutense de Madrid, p 123
[21] Pulido E, Navarro I and Hernando A 1992 *IEEE Trans. Magn.* 2424
[22] *PDF Database* 1994 JCPDS—International Center for Diffraction Data, PA (USA)
[23] Hono K, Hiraga K, Wang Q, Inoue A and Sakurai T 1992 *Acta Metall. Mater.* **40** 2137
[24] Slawska-Waniewska A, Nowicki P, Lachowicz H K, Gorria P, Barandiarán J M and Hernando A 1994 *Phys. Rev.* B **50** 6465